P700

SUOMI NPP/JPSS CROSS-TRACK INFRARED SOUNDER (CRIS): INTERCALIBRATION WITH AIRS, IASI, AND VIIRS

Dave Tobin*, Hank Revercomb, Bob Knuteson, Fred Best, Joe Taylor, Dan Deslover, Lori Borg, Chris Moeller, Graeme Martin, Ralph Kuehn, Greg Quinn, Ray Garcia and the UW PEATE Team

University of Wisconsin-Madison, Madison, Wisconsin

1. INTRODUCTION

A key part of the Calibration/Validation efforts for the Cross-track Infrared Sounder (CrIS) (e.g. Tobin et al, 2012; Revercomb et al., 2013) is the intercalibration of CrIS with the Atmospheric Infrared Sounder (AIRS) on EOS Aqua and with the Infrared Atmospheric Interferometer Sounder (IASI) on METOP-A. The spectral and radiometric accuracy goals of CrIS are very strict, and these in-orbit comparisons provide one way to assess the performance of CrIS at the order 0.1K brightness temperature level.

This paper includes sample results of the CrIS/IASI/AIRS comparisons, as well as comparisons of CrIS with the collocated imager on Suomi-NPP, VIIRS.

2. CRIS/AIRS INTERCOMPARISON RESULTS

CrIS/AIRS comparisons have been very useful in the first year of Suomi-NPP due to the large yield due to the similar orbits of Suomi-NPP and Aqua, and because a large number of validation studies have been performed to date on the AIRS data making it a known quantity for evaluating the more recent CrIS data. The AIRS/CrIS intercomparison method and sample results are presented using Figures 2.1 through 2.7.

The intercomparison technique involves collecting the CrIS and AIRS data found within 100km of the Simultaneous Nadir Overpass (SNO) locations that occur with +/- 20 minute simultaneity. A sample of this is shown on the left hand side of Figure 2.1. For each such case, the mean and standard deviation of the radiance spectra are recorded for both CrIS and AIRS. The right hand side of Figure 2.1 shows an important result: for a large ensemble of SNOs the spatial collocation errors of this analysis approach are random and gaussianly distributed, according the spatial variability of the scenes, and unbiased. The full distribution for all scenes is the sum of many gaussians. This leads to a simple yet powerful and accurate method for computing biases between the two sensors where a weighted mean difference between the two sensors is computed, using the spatial variability of each SNO to provide the weights. The uncertainty in the weighted mean differences is also computed. This is done independently for each spectral channel after performing spectral manipulations to account (as much as possible) for the differences in the spectral responses of CrIS and AIRS.

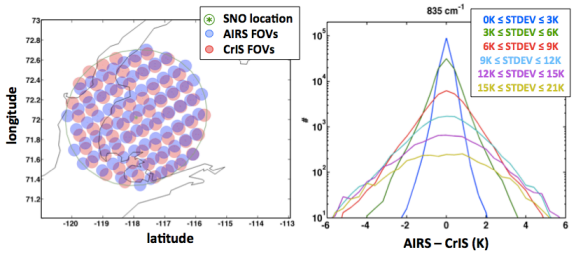

Figure 2.1. A sample CrIS/AIRS SNO (left hand side) and the distribution of 835 cm-1 brightness temperature differences for various ranges of spatial variability for a large ensemble of SNOs (right hand side).

Because Suomi-NPP and EOS Aqua are in similar orbits, there are many SNOs distributed over a wide range of latitude and longitude. Collocations collected between 25 Feb and 18 Dec 2012 are shown in Figure 2.2. This includes "SNOs" for view angles less than or equal to 30 degrees and CrIS/AIRS view angle

*Corresponding author address: David C. Tobin, Univ. of Wisconsin-Madison, Space Science and Engineering Center, 1225 West Dayton Street, Madison, WI 53705; e-mail: dave.tobin@ssec.wisc.edu

differences less than 3 degrees (i.e. not just pure nadir cases). AIRS data is L1B v5 and CrIS data is calibrated using ADL/CSPP v1.1 with native engineering packet contents.

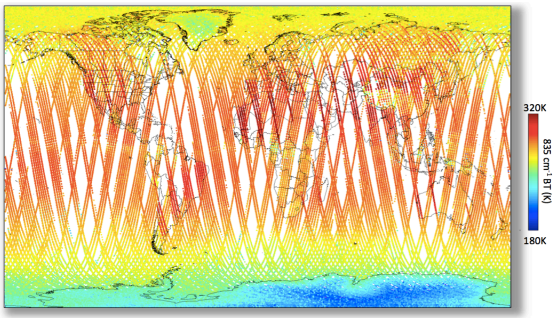

Figure 2.2. The spatial map of 598,083 CrIS/AIRS SNOs collected between 25 Feb and 18 Dec 2012. Scan angles ≤ 30°; Scan angle difference ≤ 3°; Time Diff <= 20 min. AIRS data is L1B v5; CrIS data is ADL (CSPP v1.1) with native Eng. Packets.

Due to the imprecise methodology for normalizing the spectral response functions of CrIS and AIRS, and due to the time dependent variations in the AIRS spectral calibration, the comparisons shown here are limited to 10 wavenumber averages. This averaging minimizes these issues and produces a more meaningful assessment of the radiometric differences between CrIS and AIRS. The sample wavenumber regions chosen are shown in Figure 2.3. These regions include opaque and more transparent regions of each spectral band of CrIS, and include sensitivity to various components of the CrIS radiometric calibration. For example, the longwave CO_2 region is most sensitive to the longwave band nonlinearity correction (see Knuteson et al., 2013) while the longwave window is most sensitive to the CrIS Internal Calibration Target (ICT) temperature. Similarly the 1590 cm^{-1} and 2500 cm^{-1} regions have sensitivity to the CrIS ICT environmental model. AIRS, of course, also has sensitivity to its own calibration issues in as well.

Using this approach and data, sample results are shown in Figures 2.4 through 2.7. These sample results show that the radiometric agreement between CrIS and AIRS is very good – less than ~0.1K (Figure 2.5). The differences are also very stable with time (Figure 2.6), and do not show large dependence on scene brightness temperature (Figure 2.7).

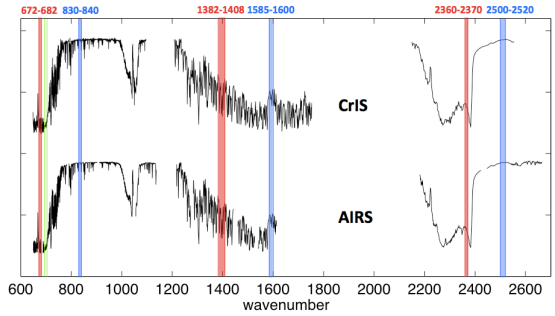

Figure 2.3. Sample CrIS and AIRS brightness temperature spectra and sample, representative wavenumber regions for the comparisons shown in Figures 2.4 through 2.7.

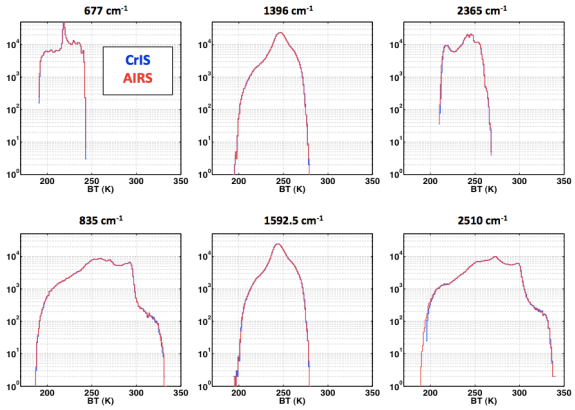

Figure 2.4. Log-scale brightness temperature distributions of CrIS and AIRS for the wavenumber regions shown in Figure 2.3.

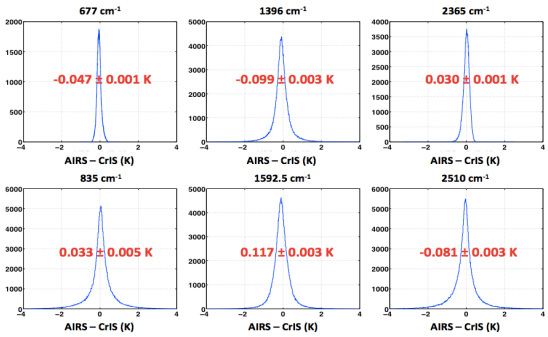

Figure 2.5. Distributions of brightness temperature differences, with mean differences and uncertainties in the mean listed in red.

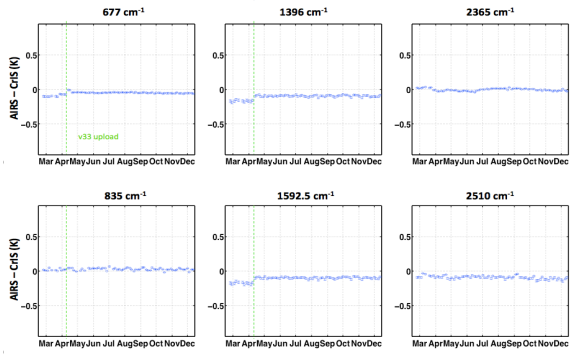

Figure 2.6. Time series of CrIS/AIRS differences. The discontinuity in mid April is due to an update of the CrIS calibration coefficients at that time.

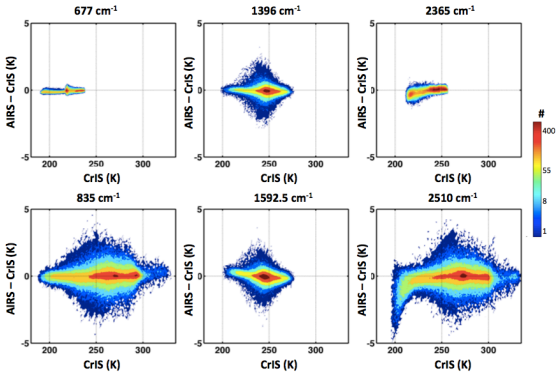

Figure 2.7. Log-scale distributions of brightness temperature differences as a function of scene brightness temperature. Dark blue is one count (one SNO) and dark red is 400.

3. CRIS/IASI INTERCOMPARISON RESULTS

The same basic methodology described for comparing CrIS and AIRS is also used for comparing CrIS and IASI. However, due to different orbits, the CrIS/IASI collocations only occur at high latitudes, and here only nadir cases are included. Additionally, because the spectral resolution differences of CrIS and IASI can be rigorously accounted for, the comparisons are shown here for the complete spectrum of CrIS. These comparisons are therefore sensitive to both the radiometric and spectral characteristics of CrIS (and IASI).

The latitude and time dependence of the CrIS/IASI SNOs are shown in Figure 3.1. The SNOs occur at latitudes of +/- 72.4 degrees. For time simultaneity of +/- 20 minutes the SNOs occur for periods of ~20 days separated by ~30 day gaps. The ensemble used here includes 2203 cases collected between March and November of 2012.

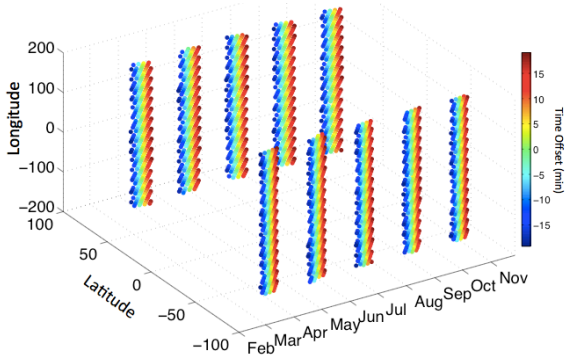

Figure 3.1. Latitude and time dependence of the CrIS/IASI SNOs, and color-coded by the SNO time difference.

Using this ensemble of SNOs, the weighted mean CrIS/IASI differences and uncertainties are shown in Figures 3.2 and 3.3 for the Northern and Southern SNOs, respectively. The overall agreement between CrIS and IASI is very good – less than a few tenth K for the large majority of channels. These comparisons use a Hamming apodization to suppress a known artifact in the current CrIS products – additional spectral (Gibbs effect) ringing in the CrIS spectra. This is a topic of current investigation of the CrIS Cal/Val team. Additionally, larger deviations are seen between CrIS and IASI for very cold scene temperatures in portions of the shortwave spectral band. These artifacts are also seen in comparisons with AIRS and in clear sky obs-calcs, and is also a topic of current investigation by the Cal/Val team.

Lastly, the FOV dependence of the CrIS/IASI differences is shown in Figure 3.4. The FOV dependence of the differences is very small – significantly less than 0.1K for the majority of spectral channels.

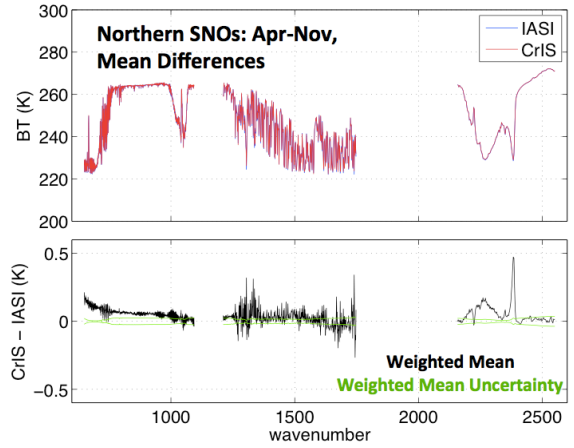

Figure 3.2. Mean spectra, weighted mean differences, and uncertainties for Northern CrIS/IASI SNOs.

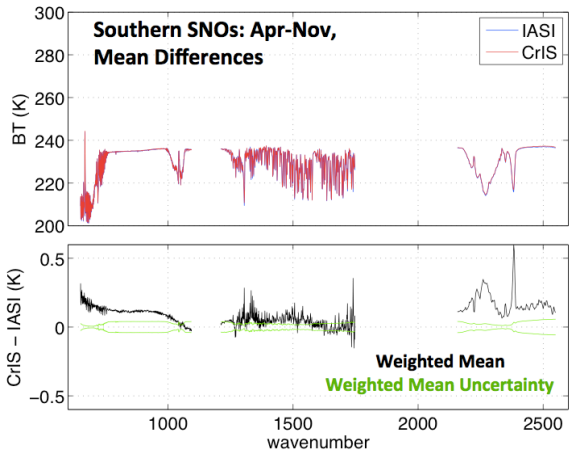

Figure 3.3. Same as Figure 3.2 but for Southern CrIS/IASI SNOs.

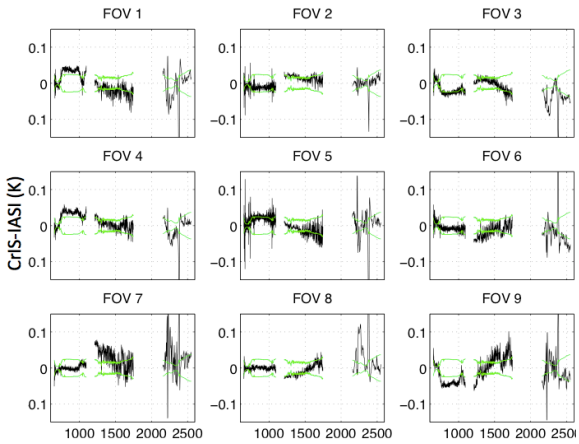

Figure 3.4. Northern CrIS/IASI SNO differences (weighted mean difference in black; weighted mean difference uncertainty in green) for each CrIS FOV.

4. CRIS/VIIRS INTERCOMPARISON RESULTS

Analogous to prior comparisons of AIRS and MODIS on EOS Aqua (Tobin et al, 2006), here we present results of intercomparing CrIS and VIIRS on Suomi-NPP. A sample CrIS spectrum and the VIIRS Spectral Response Functions (SRFs) are shown in Figure 3.1. Using VIIRS bands where CrIS provides spectral coverage, the comparisons are computed for VIIRS bands M13 (4μm), M15 (10.8μm), and M16 (12μm). It should be noted, however, that VIIRS bands M15 and M16 SRFs include an out-of-band (OOB) contribution in the gap in the CrIS spectra at ~9μm.

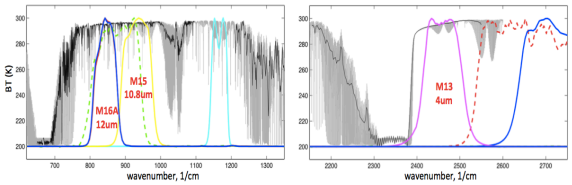

Figure 3.1. Sample monochromatic (grey) and CrIS spectra (black) overlaid with VIIRS SRFs.

Comparisons of CrIS and VIIRS are performed by, for each CrIS footprint/spectrum, convolving the CrIS spectrum with the VIIRS SRFs and computing the mean VIIRS radiances (and standard deviation) with the CrIS footprint. Spatially uniform scenes are then selected and differences between CrIS and VIIRS are computed. A sample set of data for descending node data for VIIRS M15 is shown in Figure 3.2. This results in approximately 500,000 collocated footprints suitable for comparison every day.

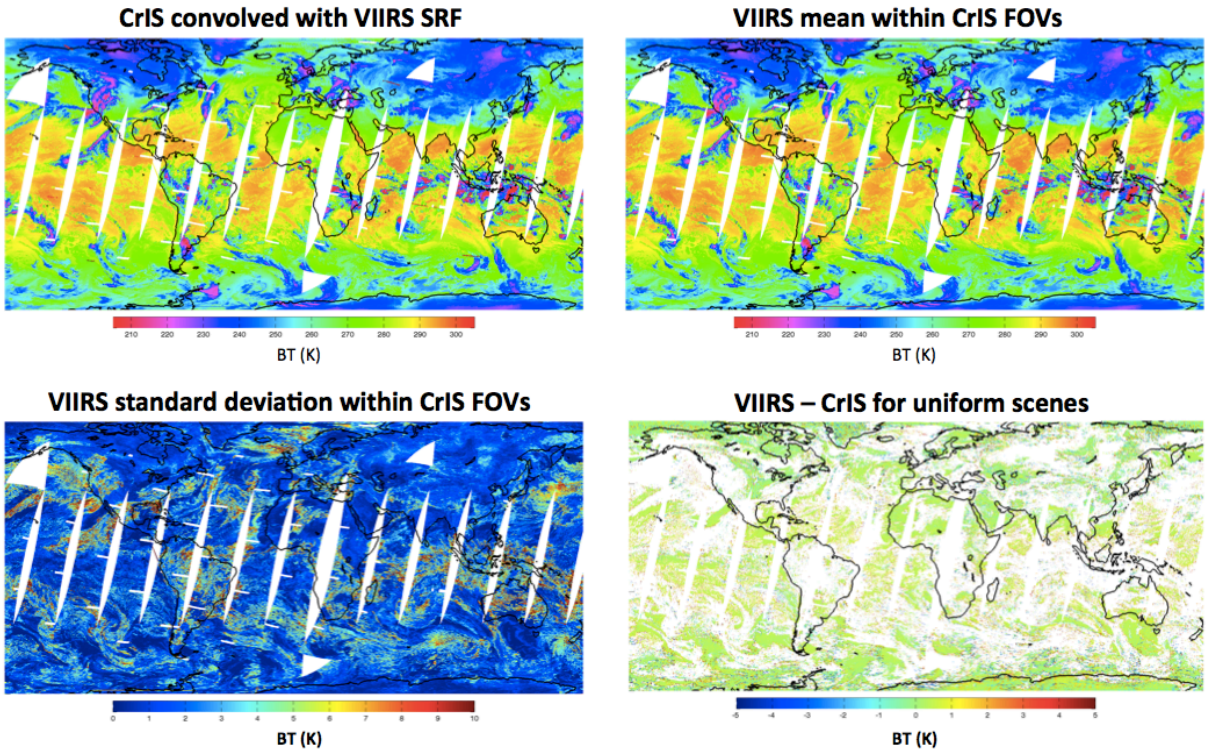

Figure 3.2. Sample comparisons of CrIS and VIIRS M15 for descending node (nighttime) data on 25 February 2012.

Using this approach, sample results are shown in Figures 3.3 through 3.6. Figure 3.3 shows the time dependence of daily mean differences. The mean differences are less than 0.1K and are very stable with time. Larger deviations in the March/April time frame are due to sensor/calibration configuration changes at that time. VIIRS nonlinearity tests, performed quarterly, are evident in the time series.

Figure 3.4 shows the scene temperature dependence of the CrIS/VIIRS differences. Bands M13 and M16 show little (less than ~0.1K) dependence on scene temperature while band M15 shows a stronger dependence on scene temperature, with differences approaching -0.4K for 200K scenes. A small portion of this difference could be due to the VIIRS OOB SRF. It is very unlikely that CrIS could have significantly different scene temperature dependence between 12μm (M16) and 10.8μm (M15). These differences are under investigation by both the CrIS and VIIRS teams.

The scan angle dependence of the CrIS/VIIRS differences is shown in Figure 3.5. This dependence is very small.

Finally, the time dependence of the CrIS/VIIRS differences during one of the VIIRS nonlinearity characterization tests is shown in Figure 3.6. During this test, the VIIRS calibration blackbody (OBC) temperature is allowed to cool from a nominal value of ~292K to below 270K. When this occurs, the agreement between the three VIIRS bands improves, and the agreement between CrIS and VIIRS improves. This general behavior is also seen for the other on-board nonlinearity tests. This implies that further improvement in the VIIRS calibration is possible, with refinements to the OBC temperature and/or background instrument temperatures. Note the period nature of the larger M15 band differences; this is due colder scene temperatures at the pole crossings as discussed with Figure 3.4.

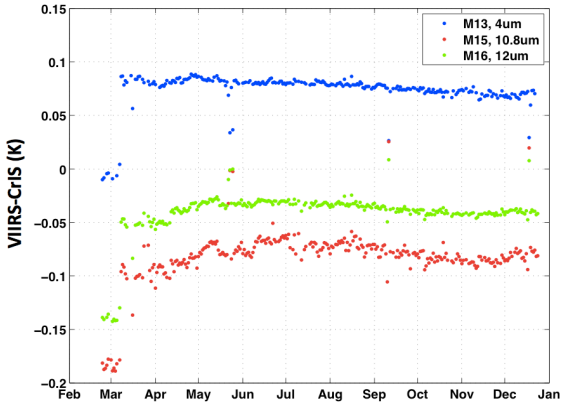

Figure 3.3. Time dependence of daily mean CrIS/VIIRS differences.

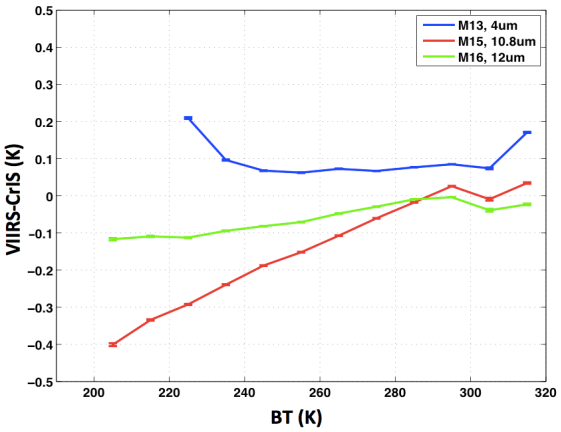

Figure 3.4. Scene temperature dependence of the CrIS/VIIRS differences.

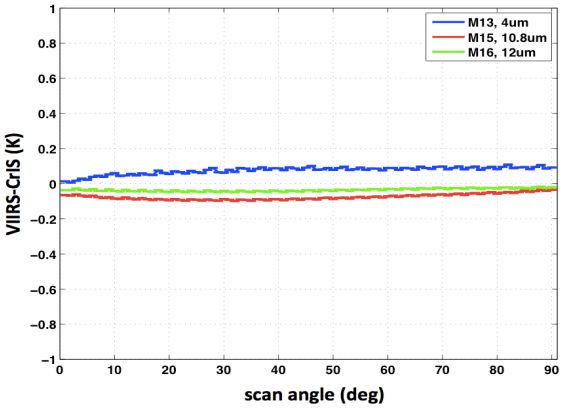

Figure 3.5. Scan angle dependence of the CrIS/VIIRS differences.

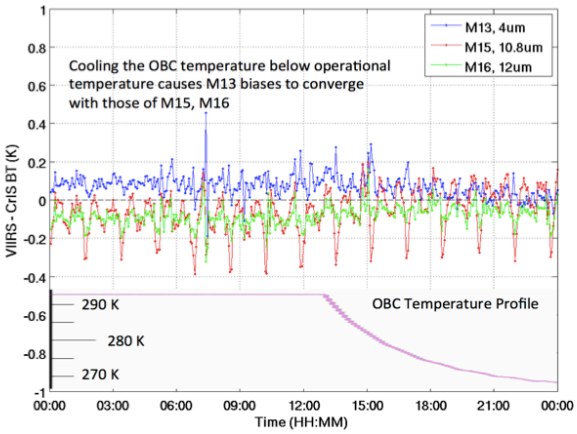

Figure 3.6. CrIS/VIIRS differences and the VIIRS OBC temperature as a function of time during a VIIRS nonlinearity characterization test.

5. SUMMARY

Intercalibration is an important tool for satellite Cal/Val efforts. This paper has presented the methodology and sample results of intercalibration of CrIS with AIRS, IASI, and VIIRS. Overall, the results show that the spectral and radiometric calibration of CrIS is very good, and issues requiring further investigation have been diagnosed. Additionally, CrIS/VIIRS comparisons show very good agreement, and yet also suggest even better agreement can be obtained with small refinements to the VIIRS calibration.

6. REFERENCES

Tobin et al., (2012), Cross-track Infrared Sounder (CrIS) Spectral Radiance Calibration and Evaluations, American Institute of Physics, in press.

Revercomb et al., 2013, Suomi NPP/JPSS Cross-track Infrared Sounder (CRIS): Radiometric and Spectral Performance, AMS Annual Meeting, Austin, TX, January 2013.

Knuteson et al., 2013, Suomi NPP/JPSS Cross-track Infrared Sounder (CRIS): Nonlinearity and On-orbit Monitoring, AMS Annual Meeting, Austin, TX, January 2013.

Tobin et al, (2006), Use of Atmospheric Infrared Sounder high–spectral resolution spectra to

assess the calibration of Moderate resolution Imaging Spectroradiometer on EOS Aqua, J. Geophys. Res., 111, D09S05, doi:10.1029/2005JD006095.

Acknowledgements: We are pleased to recognize that the on-orbit calibration and validation of the Suomi NPP CrIS has been organized under the leadership of Dr. Yong Han and has included the efforts of several organizations. Our efforts have been supported by NOAA under cooperative agreement NA10NES4400013 and also by NASA under grant numbers NNX11AK21G and NNX12AG68G.